This is a repository copy of *The addition of synthesized hydroxyapatite and fluorapatite nanoparticles to a glass-ionomer cement for dental restoration and its effects on mechanical properties*.

White Rose Research Online URL for this paper:
http://eprints.whiterose.ac.uk/104868/

Version: Accepted Version

Article:
Barandehfard, F., KianpourRad, M., Hosseinnia, A. et al. (5 more authors) (2016) The addition of synthesized hydroxyapatite and fluorapatite nanoparticles to a glass-ionomer cement for dental restoration and its effects on mechanical properties. Ceramics International. ISSN 0272-8842

https://doi.org/10.1016/j.ceramint.2016.08.122

Reuse
Unless indicated otherwise, fulltext items are protected by copyright with all rights reserved. The copyright exception in section 29 of the Copyright, Designs and Patents Act 1988 allows the making of a single copy solely for the purpose of non-commercial research or private study within the limits of fair dealing. The publisher or other rights-holder may allow further reproduction and re-use of this version - refer to the White Rose Research Online record for this item. Where records identify the publisher as the copyright holder, users can verify any specific terms of use on the publisher's website.

Takedown
If you consider content in White Rose Research Online to be in breach of UK law, please notify us by emailing eprints@whiterose.ac.uk including the URL of the record and the reason for the withdrawal request.

eprints@whiterose.ac.uk
https://eprints.whiterose.ac.uk/

The Addition of Synthesized Hydroxyapatite and Fluorapatite Nanoparticles to a Glass-Ionomer Cement for Dental Restoration and its Effects on Mechanical Properties

F. Barandehfard[a], M. Kianpour Rad[b], A. Hosseinnia[b], K. Khoshroo[c], M. Tahriri[c, d, e,], H.E. Jazayeri[c], K. Moharamzadeh[c, f], L. Tayebi[c, g, h]

[a] Nanomaterials Department, Materials and Energy Research Center (MERC), Tehran, Iran
[b] Environmental and Energy Research Group of Materials and Energy Research Center (MERC), Tehran, Iran
[c] Marquette University School of Dentistry, Milwaukee, WI, 53201 USA
[d] Dental Biomaterials Group, School of Dentistry, Tehran University of Medical Sciences (TUMS), Tehran, Iran
[e] Biomaterials Group, Faculty of Biomedical Engineering, Amirkabir University of Technology, Tehran, Iran
[f] School of Clinical Dentistry, University of Sheffield Claremont Crescent, Sheffield, S10 2TA UK
[g] Biomaterials and Advanced Drug Delivery Laboratory, School of Medicine, Stanford University, Palo Alto, CA, USA
[h] Department of Engineering Science, University of Oxford, Oxford, OX1 3PJ UK

Abstract

The objective of this study was to evaluate the effect of the addition of synthesized hydroxyapatite (HA) and fluorapatite (FA) nanoparticles to a glass-ionomer cement (GIC) on the mechanical properties, while preserving their unique and potent clinical properties. Bioceramics, such as HA and FA, have been recognized as restorative materials (e.g. GICs) in dentistry due to their chemical and biological compatibility with human hard tissues, which are considered calcium phosphate complexes. In this study, both of these inorganic nanoparticles (HA and FA) were synthesized *via* a wet-chemical precipitation method. The obtained nanoparticles were characterized with X-ray diffraction (XRD), inductively coupled plasma

atomic emission spectroscopy (ICP-AES), Fourier transformed infrared spectroscopy (FTIR), scanning electron microscopy (SEM), transmission electron microscopy (TEM) and Brunauer-Emmett-Teller (BET) Theory. Then, HA and FA were incorporated into the powder component of the resin-modified cement (Fuji II, GC gold label, GC international, Tokyo, Japan) at 5% and 8 wt%, and unblended powder was employed as control. Compressive strength (CS) and diametral tensile strength (DTA) before and after 1, 7 and 28 days of storage in distilled water were evaluated using a universal testing machine. Surface microhardness after 1 and 7 days of storage in distilled water was determined using Vickers microhardness tester. Setting and working time was measured as specified in the ASTM standard. The surface morphology of the modified GICs was examined using SEM observations. The morphology of the synthesized HA and FA nanoparticles was hexagonal, and their average sizes were about 25 nm and 30 nm, respectively. The mechanical results of the modified GICs ascertained addition of HA and FA (5 and 8 wt%) into the glass ionomer cement after 7 days of storage in distilled water exhibited statistically higher CS of about 107-113.6 MPa and 111-117.8 MPa, respectively, and also higher DTS, 13-16 MPa and 14-19 MPa, respectively. The hardness of the glass ionomers containing HA and FA nanoparticles (5 wt%) were increased by 2.21 % and 11.77%, respectively. In addition, working time and setting time by adding the 5% nanoparticles were reduced about 8.5% and 13.23 % for HA and 10.63% and 19.11 % for FA, respectively. It was concluded that glass ionomer cements containing nanobioceramics (HA and FA) are promising restorative dental materials with improved mechanical properties. These experimental GICs may be potentially employed for higher stress-bearing site restorations, such as Class I and II restorations.

Keywords: Glass ionomer cement; Hydroxyapatite; Flourapatite; Nanoparticles; Mechanical properties

1-Introduction

The glass-ionomer cements (GICs) are water-based materials that set by an acid-base reaction between a polyalkenoic acid and a fluro alumino silicate glass (1-3). Glass-ionomer cements could be employed in an extensive range of clinical applications because of their ability to revise their physical characteristics by changing the powder/liquid ratio or chemical formulation (4). Moreover, by addition of a fluorine ion, they display an anticariogenic potential, and they have appropriate biocompatibility and chemical adhesion to mineralized tissue (5-9). Nevertheless, GICs are brittle and have poor mechanical characteristics, including low fracture strength, fracture toughness and wear resistance. These properties are their main disadvantages, which limit their wide range of use in dentistry as a filling material in stress-bearing applications (9).

A number of efforts to boost the mechanical characteristics of GICs have been made in various aspects. The added components that are in the forcing phase must be accounted for, such as metal particles or zirconia, alumina, glass and carbon fiber and HA (10, 11).

Hydroxyapatite (HA) has extensively been used in biomedical and dental applications because of its similarity to major mineral components of hard tissues of the human body, such as bone and dental enamel, and their resemblance in bioactivity, biocompatibility and low solubility in moist medias (12, 13). The hydroxyapatite, due to high solubility, could efficiently fill the micro-pores present in enamel defects by liberation of inorganic ions, like calcium and phosphate, enhance resistance to de-mineralization and boost the bond strength of restorative

materials (14-33). There are different methods for synthesizing HA and FA nanoparticles, such as chemical precipitation (18, 34-36), mechanochemical (37), sol-gel (36, 38-40), hydrothermal and solvothermal (13, 41-44), sonochemical (45, 46), spray drying (47), microwave-hydrothermal (48) and biomimetic deposition methods (49-52).

Chemical bonding to tooth substrates in combination with the fluoride-releasing, low coefficient of thermal expansion, the excellent biocompatibility and strong adherence to tooth structure confers upon glass-ionomer cements (GICs) an important role in dentistry (53-56). However, the limitations of GICs are their shortage of strength and toughness and sensitivity to initial desiccation and moisture (13, 53). In other words, the acid–base setting reaction of the GICs still compromises their initial wear and early strength (56). The setting reaction is a continuous process confirmed by the enhancement of mechanical characteristics of the cement with time. Therefore, the premature exposure to water causes swelling, weakening, and leaching of ions, whereas the loss of water causes shrinkage and cracking (56).

The incorporation of a sufficient amount of HA whiskers and granules could enhance the flexural strength and improve the microstructure of GIC. It is then envisaged that the presence of HA, regardless of its morphology, in the GIC matrix could improve the mechanical characteristics of the cement without compromising its inherent favorable characteristics(13).

GICs have been discovered to interact with HA through the carboxylate groups in the polyacid. Thus, the addition of HA to GICs could not only improve the biocompatibility of GICs but also have the potential of increasing the mechanical characteristics. Additionally, it has the ability to enhance the bond strength to tooth structure because of its similar composition and

structure to enamel and dentin (12). Gu et al. reported that GICs containing 4 wt% HA particles showed increased mechanical properties in comparison with commercial GICs (57, 58).

Hence, the aim of this research was to synthesize nanohydroxyapatite and nanofluorapatite *via* a wet chemical precipitation method for addition to the powder of the restorative glass ionomer to assess the effect of these nano compounds on the mechanical characteristics and the working and setting times of the dental glass ionomer cement. It is noticeable that Fuji II GIC was employed as the control group in this research due to its availability and popularity in dental communities.

2. Materials and methods

2.1. Materials

Commercial grade glass powder and the liquid (Fuji II, GC gold label, GC international, Tokyo, Japan) were used for cement preparation. All the chemicals in this research were of analytical grades and applied as obtained from Merck Chemical Company (Germany). Hydrated calcium nitrate [$Ca(NO_3)_2.4H_2O$], diammonium hydrogen phosphate [$(NH_4)_2HPO_4$], ammonium fluoride (NH_4F), absolute ethanol (C_2H_5OH) and ammonium hydroxide (NH_4OH) were employed.

2.2. Synthesis of HA and FA nanoparticles

Initially, 84 mmol hydrated calcium nitrate ($Ca(NO_3).4H_2O$), was dissolved in 50 ml absolute ethanol, and also, another solution was made by dissolving 50 mmol diammonium hydrogen phosphate [$(NH_4)_2HPO_4$] in distilled water to make a 0.5 M solution. Both solutions were stirred to obtain transparency for 1 h. In the second step, the aqueous solution was added

drop wise at a rate of 5 ml min^{-1} to alcoholic solution with vigorous stirring. The pH of the solution was regulated to 10 by drop wise addition of NH_4OH solution. An obtained milky and gelatinous precipitate was then stirred at ambient temperature for 1 h.

In order to synthesize FA, to the solution of hydrated calcium nitrate and diammunium hydrogen phosphate, which was made exactly as the previous step, a solution of 16.7 mmol (Ca:P:F=5:3:1) ammonium fluoride (NH_4F) was added. Again, a milky and gelatinous precipitate was formed and subsequently stirred at ambient temperature for 1 h.

The obtained precipitates were centrifuged and washed by ethanol four times, dried at 80 $^{\circ}C$ for 5 h, and subsequently grinded with mortar and pestle. Finally, the resulting fine HA and FA powders were heated to 600, 700 and 800 $^{\circ}C$ at a rate of 10 $^{\circ}C$ min^{-1} and held at this temperature for 1 h.

2.3. Characterization of HA and FA nanoparticles

2.3.1. XRD analysis

The nanopowders were analyzed with x-ray diffractometer (Philips PW 3710, Netherlands, Holland), using Cu $K\alpha_1$ radiation with a wavelength, λ, of 1.54 A°. All samples were evaluated in the 2θ angle range of 20—60° at a scanning speed of 0.04 $^{\circ}$/min and a step size of 0.02° and step time of 0.5 s. The XRD analysis was carried out on both synthesized powders (HA and FA) before and after calcination.

2.3.2. FTIR analysis

Fourier transform infrared (FTIR) spectra of the synthesized nano-HA were recorded using a VECTOR 33 FTIR spectrometer (Bruker, Germany). The samples were analyzed in the range of 4000-400 cm^{-1} at $4cm^{-1}$ resolution after averaging 50 scans to examine the chemical functional groups.

2.3.3. AES-ICP analysis

A Perkin-Elmer Optima-3000 was employed to determine the chemical composition of the HA and FA nanoparticles by atomic emission spectroscopy-inductively coupled plasma analysis (AES-ICP).

2.3.4. BET analysis

The specific surface area of the resulting powders was assessed by Brunauer–Emmett–Teller (BET) technique (Bel Sorp miniII, Japan), using N_2 as an adsorption gas.

2.3.5. SEM observations

HA and FA nanoparticles were examined by scanning electron microscopy (SEM; VEGA\\TESCAN Czech Republic), which was operated at 15 KeV. The samples were prepared by dispersing a thin layer of the powders on an aluminum substrate and then coated with gold to support an electric conduction of the surface of the samples.

2.3.6. TEM observations

The morphology of the samples was evaluated using transmission electron microscopy (TEM; FEG, Philips, 200 Kv). For this purpose, the samples were prepared by dispersing a few drops of HA and FA on carbon film supported by copper grids. Particle size measurement was conducted using Clemex Image Analyzer software.

2.4. Formulation and characterization of the modified glass ionomer cements

2.4.1. Preparation of samples

In order to prepare nano HA and nano FA-containing glass powders, an appropriate amount of glass ionomer powder in combination with either nano HA or nano FA was accurately weighed and blended for 30 min. The commercial glass powder was Fuji II GIC and a powder/ liquid (P/L) ratio of 2.7/1 was employed as recommended by the manufacturer. The GIC samples were blended and produced at ambient temperature according to the manufacturer's instructions.

Cylindrical samples were fabricated using PTFE cylindrical molds with a 6 mm diameter and 12 mm height for a compressive strength (CS) test, and the samples were also fabricated for a 6 mm diameter and a 3 mm height for diametral tensile strength test (DTS) (51). The molds were filled with the material and covered with PTFE tape and glass slides, flattened and pressed in order to eliminate air bubbles from unset cement paste. The samples were ejected from the molds after 30 min and stored in distilled water at 37 ºC and 100% humidity for 1, 7 and 28 days in an incubator until testing time. Four samples (n=6) were made for each test.

2.4.2. XRD analysis

XRD patterns of the prepared modified glass-ionomer cements were obtained at room temperature using a Philips PW 3710 (Cu-K_α radiation) with a wavelength, λ, of 1.54 A°. The samples were analyzed in the 2θ angle range of 15–60°, and their patterns were studied to determine the crystal phases present in the samples.

2.4.3. SEM observations

The prepared modified glass-ionomer cement samples were coated with a thin layer of Gold (Au) by sputtering (EMITECH K450X, England), and then, the surface morphology of the cement samples were observed in a scanning electron microscope (SEM; VEGA\\TESCAN Czech Republic) that operated at an acceleration voltage of 15 kV.

2.4.4. Mechanical properties

Mechanical tests were carried out on a screw-driven mechanical testing machine (SANTAM, STM 20) with an across head speed of 0.5 mm min^{-1} until failure occurred. The compressive strength and diametral tensile strength are common tests to assess the mechanical properties of glass ionomers.

2.4.5. Micro hardness test (Vickers)

A micro hardness test of the samples was carried out by a Vickers micro hardness tester (Akashi, MVK-H21, Japan). This test was performed with 50 g load applied for 15 s using a diamond indenter.

2.4.6. Setting and working time

The setting time is the time when the cement paste loses its plasticity and starts to harden to form a solid mass. Setting time of the prepared cements was measured using a Vicat test according to the ASTM-C-18798 standard. The setting time was collected as the time passed between the end of mixture to when the needle failed to make a complete circular indentation(59, 60).

2.5. Statistical analysis

Statistical analysis was carried out using SPSS software. One-way analysis of variance (ANOVA) and Tukey test were performed to determine statistically significant differences between the experimental groups. Statistical significance was obtained at $p < 0.05$. Error bars indicate the standard deviation of the mean value.

3. Results and discussion

3.1. Characterization of synthesized HA and FA

3.1.1. XRD analysis

The XRD patterns of the synthesized HA and FA nanoparticles at 20 ºC and calcinations at 600, 700 and 800 ºC are given in Fig. 1a and b, respectively. As it can be observed, the resulting pattern of the samples before calcinations displayed the presence of amorphous and crystalline phases simultaneously. Checking with the related card of the pure material, it was

exhibited that the synthesized nanoparticles after calcination at 700 °C were formed in almost pure states (ICDD standard, HA: JCPDS No. 09-0432), and all the peaks corresponded to a hexagonal crystal system of HA(42, 43, 61-65). In all cases, the small size of the particles formed after drying caused the formation of broad peaks in the XRD pattern(66). The crystal size of nano HA is determined to be about 16.9 nm by using Rietveld software and the Scherrer equation for (002) peak, and the crystal structure that is hexagonal is consistent with the TEM observations.

Also, checking with the related card of the pure material, it was found that the nanoparticles after calcination at 700 °C were formed in almost pure states (ICDD standard, FA: JCPDS No. 03-0736), and all the peaks corresponded to a hexagonal crystal system of FA (14). The crystal size of nano FA is determined to be approximately 22.5 nm by using Rietveld software and the Scherrer equation for (002) peak, and the crystal structure is hexagonal, affirming the TEM observations.

The peaks of HA at (211) and (112) tend to merge due to fluoridation(67, 68). Additionally, the XRD results revealed that they have a high degree of crystallinity due to the incorporation of fluorine. The slight shift of (300) to the right side of 2θ axial leads to a decrease of the parameter (a) in the crystalline structure of FA(68, 69).

Table 1 confirmed that FA peaks are sharper than HA peaks; therefore, the presence of flouride in the structure of HA instigates an increase in the crystallinity of FA that is responsible for the chemical and thermal stability of FA. In addition, using Retvield software, the crystal size and structure of the resulting nano HA and FA were determined and presented in Table 1. The data in the table indicates that the crystals obtained from HA and FA are formed as hexagonal

structures that have a crystal size of 16.9 and 22.5, respectively. According to the results, the samples that were calcined at 700 ºC have the most optimum characteristics; thus, the mentioned sample was selected as the optimum sample, and other analyses were carried out on it.

(Figure 1)

(Table 1)

3.1.2. FTIR analysis

The FTIR spectra of HA and FA powders after calcination at 700 ºC are shown in Figs. 2a and b. In the analysis, mainly the peaks from PO_4^{3-} and OH^{-1} groups in the hydroxyapatite and fluorapatite can be recognized. In FTIR spectra of nano HA, the IR bands observed at 1097, 1056 and 985 cm^{-1} are due to the phosphate stretching vibration, and the bands at 601, 570 and 467 cm^{-1} belong to the phosphate bending vibration. The bands appearing at 634 and 3571 cm^{-1} ascertain the presence of bending and stretching hydroxyl ion vibration, respectively.

In FTIR spectra of nano FA, the IR bands observed at 983, 1053 and 1103 cm^{-1} are due to the phosphate stretching vibration, and the bands at 474, 578 and 603 cm^{-1} belong to the phosphate bending vibration (70).

Sushananek et. al reveals the disappearing of the peaks at 3571 and 631 cm^{-1} that are related to the presence of bending and stretching hydroxyl ion vibration in the FA sample, which affirms the formation of FA (70). Also, the peak at 754 cm^{-1} demonstrated that hydroxyl groups in the apatite structure are replaced and saturated with fluorine (71).

IR bands of HA spectra are in complete accordance with previous research studies that have been conducted by Moshavernia et. al (53), Philips et. al (67), Redy et. al (72) and Nike et. al

(73). In addition, an OH band in HA spectra disappeared in the FA spectra and was replaced by a broad peak in the region of 900-1100 ºC that is in accordance with the research of Wei et. al (53, 68).

When hydroxyl groups were relatively substituted with fluoride ions in hydroxyapatite, the stretching mode of OH^- could move to the new band that arises from OH….F bond. It is worth mentioning that OH^- bands were completely removed in FA, proposing that the substantial amount of fluoride ions were replaced with hydroxyl groups.

Finally, the peak assignments of FTIR spectra of synthesized HA and FA particles divulged purity of the final product.

(Figure 2)

3.1.3. ICP-AES analysis

The result of measurement of elemental composition (Ca and P content) and Ca/P molar ratio for HA and FA are summarized in Tables 2 and 3, respectively. The Ca/P molar ratio was found to be 1.66 and 1.65 for HA and FA, respectively. These results revealed that nano HA and FA that were calcined at 700 º C have an approximately stoichiometric composition.

(Table 2)

(Table 3)

3.1.4. BET analysis

Table 4 shows the BET results of calcined nano HA and FA at 700 °C. BET results provide an important indication about the particle sizes and specific area of the nano powders.

(Table 4)

3.1.5. SEM observations

SEM micrographs of HA and FA nanoparticles are shown in Fig. 3a and b, respectively. These micrographs ascertained that the morphology of all of the nanopowders were spherical and semi spherical shape. HA and FA nanoparticles formed at 700 ºC displayed a particle size of about 30 and 38 nm, respectively.

It can also be noted from the figures that both of the particles have the tendency to aggregate.

(Figure 3)

3.1.6. TEM observations

The TEM micrograph and the selected area electron diffraction (SAED) pattern of the calcined HA and FA nanoparticles are shown in Figs. 4a, b and Figs .5a and b, respectively. It can be noted that the calcined HA and FA have an ellipsoid-like morphology. The crystallite size of the calcined nano HA and FA was estimated from TEM micrographs by image analysis using Clemex software, which has an estimated mean crystallite size of about 24 nm and 30 nm, respectively. The SAED patterns confirm the formation of hexagonal HA and FA crystals, which is also in agreement with the results obtained from the XRD analysis. Furthermore, the particles

obtained from both of the methods of synthesis have a strong tendency to agglomerate, as shown in both figures.

The electron diffraction pattern of the experimentally selected area was created from reflections (spots) originating from the individual particles. All of the reflections could be marked with regard to the HA and FA structures. The reflections of the experimental pattern are attached to the rings at the positions where the determined powder electron diffraction pattern displays the highest intensity: (211) and (002) for nano HA and (213), (211) and (210) for nano FA. Those positions are indexed on the experimental diffraction pattern in Figs. 5a and b. The reflections are broadened and diffused because of the small particle size of the product.

(Figure 4)

(Figure 5)

3.1. Characterization of the modified glass ionomer cements

3.1.1. XRD analysis

The XRD patterns of the FujiII glass ionomer sample, HA-contained GIC and FA-contained GIC after mixing with poly acid are shown in Fig. 6a–c, respectively. The FujiII set cement sample (Fig. 6a) does not display any sharp or strong peaks in the XRD pattern, affirming that it is a predominantly amorphous material, whereas in the XRD patterns of both the HA-and FA-added set GICs, peaks related to the crystalline apatite structure were seen

between 20º and 45º (see Fig. 6b and c). These obtained results correlated well with those described previously by Moshavernia et. al and Milne et. al (53, 74).

(Figure 6)

3.1.2. SEM observations

SEM micrographs of the prepared GICs containing nano HA and FA are shown in Fig .7a and b and Fig. 8a and b, respectively. Considering the secondary electron images, the presence of the synthesized nanoceramics could not be easily observed, but in back scatter SEM micrographs, the distribution of nanoceramics in the cement could be seen.

(Figure 7)

(Figure 8)

3.1.3. Setting and Working time

Table 5 lists the setting and working times of the prepared control cements and cement containing the nanoceramics prepared through the wet-chemical precipitation method. The obtained results indicate that after adding the nanoceramics (HA and FA), setting and working times decreased. The nanoceramics have a higher specific area than the commercial glass powders; thus, they entered the reaction sooner than the rest of the other glass powders and caused a decrease in the setting and working times. In addition, working and setting time, by adding the nanoparticles, were reduced by about 8.5% and 13.23 % for 5% HA nanoparticles and by 10.63% and 19.11 % when 5% FA nanoparticles were added.

The presence of the nanoparticles in the cement could affect the setting reaction by the formation of more polysalt bridges in the network, and hence, it enhances the mechanical properties of the set cements.

(Table 5)

3.1.4. Mechanical properties

3.1.4.1. CS and DTS

The compressive strengths of the cements with different percentages (by weight) of nano ceramics (HA and FA) are shown in Figs. 9 and 10. As the figures show, those samples contained 8% (by weight) of the nanoceramics as compared to the control sample, and the sample that contained 5% nanoceramics show higher compressive strength. Additionally, the samples containing the nano FA in comparison with those containing nano HA display higher strength due to the higher crystallinity.

It is distinguished that during the first day of storage of the samples in distilled water, the compressive strength was the lowest because some Ca^{2+} and Al^{3+} did not react with the polymer in the liquid, but after 7 and 28 days, the reaction of the cations with carboxylate groups of the polymer was completed, and as a result, the compressive strength was enhanced. Interestingly enough, the compressive strength of the cement changed slightly after elapsing 7 days.

The compressive strength of the glass ionomer containing nanoceramics were enhanced due to the crystalline increase with the presence of nanoceramics. Therefore, the samples

containing FA, because of its higher degree of crystallinity in comparison to nano HA, the CS was enhanced more than samples containing HA.

(Figure 9)

(Figure 10)

The diametral tensile strength of the cements with different percentages of nanoceramics are shown in Figs. 11 and 12. DTS testing was developed to evaluate brittle materials with little or no plastic deformation (75). The samples contained 8% nanoceramics in comparison with the control sample, and the sample that contained 5% nanoceramics displayed a higher DTS. Additionally, the samples containing the nano FA, in comparison with the ones that contained HA, exhibited higher strength due to higher crystallinity of FA.

It was distinguished at the first day of storage in distilled water, samples demonstrated the lowest diametral tensile strength because some Ca^{2+} and Al^{3+} did not react with the polymer in the liquid, but after 1 and 7 days, they reacted with carboxylate groups and resulted in an increase in diametral tensile strength. After 28 days, no considerable change in strength was seen. These results could be due to the supplementation of HA to the glass monomer, causing a chemical reaction between polycarboxylic acid and HA and forming strong chemical bonds (62).

(Figure 11)

(Figure 12)

Results of the mechanical tests confirmed that all of the GIC samples after 1 and 7 days of storage in distilled water at 37 ºC show high compressive and diametral tensile strength. Previous research explained that nano HA is considered to be a suitable additive to GIC. Yap et.

al (76) exhibited that GIC containing 4% HA displays higher DTS and CS (CS: 172.17 MPa and DTS: 12.07 MPa) compared to the commercial GIC having no additive as a reinforcement. In the current research, in order to improve the mechanical characteristics of GICs, nano HA and FA (20-30 nm) were synthesized and added to the powders to evaluate the effect of the incorporation of the nanoparticles. The cements containing the nano FA showed higher DTS and CS in comparison to the samples containing nano HA. This might be due to stability and slow solubility of FA in distilled water. Adding the nano FA to the powder influenced the setting reaction and improved the mechanical properties of the set cement. Additionally, the small particle size of the nanoceramics led to a broad distribution of particle size and thus, the particles could have a better chance to fill vacancies and hence reinforce the cement structure. Enhancing the crystallinity of the nano HA and FA could substantiate the mechanical properties of the cement (77). It could also be concluded that the mechanical behavior of GICs containing the nanoparticles was boosted after enduring a long storage time. This is due to the formation of a salty aluminum bridge in the network. Because of small particle size and higher specific area of the synthesized nanoparticles in comparison to glass particles, it can be concluded that if the amount of these nanoparticles exceed the optimum amount it could have an adverse effect on the mechanical behavior of the set cement. The incorporation of extra nanoparticles to the glass ionomer powder could have an adverse effect on their mechanical characteristics. Incorporating excess nanoparticles could decrease the intersection between the particles and ionomer network, and thus, HA could not react with the ionomer to form the crosslinking network.

The results of strength testing confirmed that the compressive and diametral tensile strengths of those glass ionomers containing each nanoparticle after 7 days were enhanced, at most, by 3.7% and 16.66% for 5% HA nanoparticles and by 12.26% and 36.66 % when 5% FA nanoparticles were appended. Moreover, the results of strength testing confirmed that the compressive and diametral tensile strengths of those glass ionomers containing each nanoparticle after 7 days were increased, at most, by 6.19% and 28.33% for 8% HA nanoparticles and 10.37% and 52% when 8% FA nanoparticles were added.

3.1.4.2. Hardness

Table 6 lists the resulting micro hardness following the incorporation of 5 and 8% nanoceramic to the glass ionomer cements after storage in distilled water at 37º C for 1 and 7 days. Hardness is one of the most important mechanical properties of a dental material. It supplies an indication of the resistance of the material for scratching or abrasion (10). The hardness of all samples doubled after 7 days. Nanoceramic-incorporated cements show significant hardness in comparison to the control sample in each group (78).

(Table 6)

The hardness of the glass ionomers containing 8% HA and FA nanoparticles were increased by 6.32 % and 27.21%, respectively. The hardness of the glass ionomers containing 5% HA and FA nanoparticles were increased by 2.21 % and 11.77%, respectively.

The results obtained in this research were in full agreement with those obtained by Kent and Wilson, which indicated that the finer grained glasses could produce stronger cements. They revealed that the finer powder particles shorten the working time and also hasten the

setting time (79). Lastly, it is important to point out that nanoparticles, due to their higher degree of crystallinity and colloidal stability, have a greater reinforcing effect and easier application (80).

4. Conclusions

The incorporation of the synthesized nano HA and FA into Fuji II commercial GIC increased the mechanical characteristics (compressive, diametral tensile and hardness) of the resulting cements. These bioceramics are thus appraised, promising additives for glass ionomer restorative dental materials. Eventually, due to the lower solubility rate of FA, the FA-containing GICs ascertained higher values after 7 and 28 days for the mechanical tests in comparison to HA-added GIC samples.

Conflict of interest

The authors declare that they have no conflicts of interest.

References

1. Wilson AD, Kent B. A new translucent cement for dentistry. The glass ionomer cement. *British dental journal* 1972;**132**(4):133-35.
2. McLean JW, Gasser O. Glass-cermet cements. *Quintessence international (Berlin, Germany: 1985)* 1985;**16**(5):333-43.
3. Wilson AD, McLean JW. Glass-ionomer cement: Quintessence Pub Co; 1988.
4. Nicholson JW. Chemistry of glass-ionomer cements: a review. *Biomaterials* 1998;**19**(6):485-94.
5. Yip H, Tay F, Ngo H, Smales R, Pashley DH. Bonding of contemporary glass ionomer cements to dentin. *Dental materials* 2001;**17**(5):456-70.
6. Eslami H, Solati-Hashjin M, Tahriri M. The comparison of powder characteristics and physicochemical, mechanical and biological properties between nanostructure ceramics of

hydroxyapatite and fluoridated hydroxyapatite. *Materials Science and Engineering: C* 2009;**29**(4):1387-98.
7. Wang M. Developing bioactive composite materials for tissue replacement. *Biomaterials* 2003;**24**(13):2133-51.
8. Chen Q, Wong C, Lu W, Cheung K, Leong J, Luk K. Strengthening mechanisms of bone bonding to crystalline hydroxyapatite in vivo. *Biomaterials* 2004;**25**(18):4243-54.
9. Lohbauer U. Dental glass ionomer cements as permanent filling materials?–properties, limitations and future trends. *Materials* 2009;**3**(1):76-96.
10. Ab Rahman I, SAM'AN MM, Luddin N, Shiekh RA. One-pot synthesis of hydroxyapatite–silica nanopowder composite for hardness enhancement of glass ionomer cement (GIC). *Bulletin of Materials Science* 2014;**37**(2):213-19.
11. Sari MN, Tabaii ES, Vaziri AS, Ghaffari H, Kashani MA, Amirabadi GE. Effect of Nano-Hydroxyapatite Incorporation into Resin Modified Glass Ionomer Cement on Ceramic Bracket Debonding. *Journal of Islamic Dental Association of IRAN (JIDAI)* 2014;**26**(2).
12. Lucas ME, Arita K, Nishino M. Toughness, bonding and fluoride-release properties of hydroxyapatite-added glass ionomer cement. *Biomaterials* 2003;**24**(21):3787-94.
13. Sadat-Shojai M. Preparation of hydroxyapatite nanoparticles: comparison between hydrothermal and solvo-treatment processes and colloidal stability of produced nanoparticles in a dilute experimental dental adhesive. *Journal of the Iranian Chemical Society* 2009;**6**(2):386-92.
14. Eslami H, Solati-Hashjin M, Tahriri M. Synthesis and characterization of nanocrystalline fluorinated hydroxyapatite powder by modified wet-chemical process. *J Ceram Process Res* 2008;**9**:224-9.
15. Tahriri M, Solati-Hashjin M, Eslami H. Synthesis and characterization of hydroxyapatite nanocrystals via chemical precipitation technique. *Iranian Journal of Pharmaceutical Sciences* 2008;**4**(2):127-34.
16. Fatehi K, Moztarzadeh F, Solati-Hashjin M, Tahriri M, Rezvannia M, Ravarian R. In vitro biomimetic deposition of apatite on alkaline and heat treated Ti6A14V alloy surface. *Bulletin of Materials Science* 2008;**31**(2):101-08.
17. Ashuri M, Moztarzadeh F, Nezafati N, Hamedani AA, Tahriri M. Development of a composite based on hydroxyapatite and magnesium and zinc-containing sol–gel-derived bioactive glass for bone substitute applications. *Materials Science and Engineering: C* 2012;**32**(8):2330-39.
18. Eslami H, Tahriri M, Bakhshi F. Synthesis and characterization of nanocrystalline hydroxyapatite obtained by the wet chemical technique. *Materials Science Poland* 2010;**28**(1):5--13.
19. Eslami H, Solati-Hashjin M, Tahriri M. Effect of fluorine ion addition on structural, thermal, mechanical, solubility and biocompatibility characteristics of hydroxyapatite nanopowders. *Advances in Applied Ceramics: Structural, Functional and Bioceramics* 2010;**109**(4):200.
20. Poursamar SA, Rabiee M, Samadikuchaksaraei A, Tahriri M, Karimi M, Azami M. Influence of the value of the pH on the preparation of nano hydroxyapatite polyvinyl alcohol composites. *J Ceram Process Res* 2009;**10**(5):679-82.
21. Tahriri M, Moztarzadeh F. Preparation, characterization, and in vitro biological evaluation of PLGA/nano-fluorohydroxyapatite (FHA) microsphere-sintered scaffolds for biomedical applications. *Appl Biochem Biotechnol* 2014;**172**(5):2465-79.
22. Fatehi K, Moztarzadeh F, Solati-Hashjin M, Tahriri M, Rezvannia M, Saboori A. Biomimetic hydroxyapatite coatings deposited onto heat and alkali treated Ti6Al4V surface. *Surface Engineering* 2013.

23. Zamanian A, Moztarzadeh F, Kordestani S, Hesaraki S, Tahriri M. Novel calcium hydroxide/nanohydroxyapatite composites for dental applications: in vitro study. *Advances in Applied Ceramics* 2010;**109**(7):440-44.
24. Shafiei F, Behroozibakhsh M, Moztarzadeh F, Haghbin-Nazarpak M, Tahriri M. Nanocrystalline fluorine-substituted hydroxyapatite [Ca 5 (PO 4) 3 (OH) 1-x F x (0⩽ x⩽ 1)] for biomedical applications: preparation and characterisation. *IET Micro & Nano Letters* 2012;**7**(2):109-14.
25. Bizari D, Moztarzadeh F, Rabiee M, Tahriri M, Banafatizadeh F, Ansari A, et al. Development of biphasic hydroxyapatite/dicalcium phosphate dihydrate (DCPD) bone graft using polyurethane foam template: in vitro and in vivo study. *Advances in Applied Ceramics* 2011;**110**(7):417-25.
26. Masaeli R, Kashi TSJ, Dinarvand R, Rakhshan V, Shahoon H, Hooshmand B, et al. Efficacy of the biomaterials 3wt%-nanostrontium-hydroxyapatite-enhanced calcium phosphate cement (nanoSr-CPC) and nanoSr-CPC-incorporated simvastatin-loaded poly (lactic-co-glycolic-acid) microspheres in osteogenesis improvement: An explorative multi-phase experimental in vitro/vivo study. *Materials Science and Engineering: C* 2016;**69**:171-83.
27. Haghbin-Nazarpak M, Moztarzadeh F, Solati-Hashjin M, Mirhabibi AR, Tahriri M. PREPARATION, CHARACTERIZATION AND GENTAMICIN SULFATE RELEASE INVESTIGATION OF BIPHASIC INJECTABLE CALCIUM PHOSPHATE BONE CEMENT. *Ceramics–Silikáty* 2010;**54**(4):334-40.
28. Haghbin-Nazarpak M, Moztarzadeh F, Solati-Hashjin M, Tahriri M, Khoshroo K. Injectable and bioresorbable calcium phosphate delivery system with gentamicin sulphate for treatment of bone diseases: in vitro study. *Advances in Applied Ceramics* 2011;**110**(8):482-89.
29. Ravarian R, Moztarzadeh F, Hashjin MS, Rabiee S, Khoshakhlagh P, Tahriri M. Synthesis, characterization and bioactivity investigation of bioglass/hydroxyapatite composite. *Ceramics International* 2010;**36**(1):291-97.
30. Azami M, Moztarzadeh F, Tahriri M. Preparation, characterization and mechanical properties of controlled porous gelatin/hydroxyapatite nanocomposite through layer solvent casting combined with freeze-drying and lamination techniques. *Journal of Porous Materials* 2010;**17**(3):313-20.
31. Rezvannia M, Moztarzadeh F, Tahriri M. Formation of hydroxyapatite nanoneedles on the surface of a novel calcium phosphate/blood plasma proteins biocement in simulated body fluid (SBF). *Journal of Ceramic Processing Research* 2009;**10**(5):669-73.
32. Hooshmand T, Abrishamchian A, Najafi F, Mohammadi M, Najafi H, Tahriri M. Development of sol-gel-derived multi-wall carbon nanotube/hydroxyapatite nanocomposite powders for bone substitution. *Journal of Composite Materials* 2013;**48**(4):483-89.
33. Fatehi K, Moztarzadeh F, Tahriri M, Khoshroo K, Heidari S, Sadeghi A. Biomimetic Synthesis, Characterization, and Adhesion Properties of Bone-Like Apatite on Heat and Alkaline-Treated Titanium Alloy. *Synthesis and Reactivity in Inorganic, Metal-Organic, and Nano-Metal Chemistry* 2014;**44**(10):1535-40.
34. Ferraz M, Monteiro F, Manuel C. Hydroxyapatite nanoparticles: a review of preparation methodologies. *Journal of Applied Biomaterials and Biomechanics* 2004;**2**(2):74-80.
35. Monmaturapoj N. Nano-size hydroxyapatite powders preparation by wet-chemical precipitation route. *Journal of Metals, Materials and Minerals* 2008;**18**(1):15-20.
36. Guzman Vazquez C, Pina Barba C, Munguia N. Stoichiometric hydroxyapatite obtained by precipitation and sol gel processes. *Revista mexicana de física* 2005;**51**(3):284-93.
37. Nasiri-Tabrizi B, Honarmandi P, Ebrahimi-Kahrizsangi R, Honarmandi P. Synthesis of nanosize single-crystal hydroxyapatite via mechanochemical method. *Materials Letters* 2009;**63**(5):543-46.
38. Beganskienė A, Dudko O, Sirutkaitis R, Giraitis R. Water based sol-gel synthesis of hydroxyapatite. *Mater Sci (Medžiagotyra)* 2003;**9**:383-6.

39. Balamurugan A, Michel J, Faure J, Benhayoune H, Wortham L, Sockalingum G, et al. Synthesis and structural analysis of sol gel derived stoichiometric monophasic hydroxyapatite. *Ceramics- Silikaty* 2006;**50**(1):27-31.
40. Vijayalakshmi U, Rajeswari S. Preparation and characterization of microcrystalline hydroxyapatite using sol gel method. *Trends Biomater Artif Organs* 2006;**19**(2):57-62.
41. Montazeri L, Javadpour J, Shokrgozar MA, Bonakdar S, Javadian S. Hydrothermal synthesis and characterization of hydroxyapatite and fluorhydroxyapatite nano-size powders. *Biomedical Materials* 2010;**5**(4):045004.
42. Qi C, Zhu YJ, Lu BQ, Zhao XY, Zhao J, Chen F, et al. Hydroxyapatite Hierarchically Nanostructured Porous Hollow Microspheres: Rapid, Sustainable Microwave-Hydrothermal Synthesis by Using Creatine Phosphate as an Organic Phosphorus Source and Application in Drug Delivery and Protein Adsorption. *Chemistry–A European Journal* 2013;**19**(17):5332-41.
43. Wang YJ, Lai C, Wei K, Chen X, Ding Y, Wang ZL. Investigations on the formation mechanism of hydroxyapatite synthesized by the solvothermal method. *Nanotechnology* 2006;**17**(17):4405.
44. Suchanek WL, Riman RE. Hydrothermal synthesis of advanced ceramic powders. Advances in Science and Technology; 2006: Trans Tech Publ; 2006. p. 184-93.
45. Barandehfard F, Keyanpour-Rad M, Hosseinnia A, Kazemzadeh SM, Vaezi MR, Hassanjai-Roshan A. Sonochemical synthesis of hydroxyapatite and fluoroapatite nanosized bioceramics. *Journal of Ceramic Processing Research* 2012;**13**(4):437-40.
46. Yoruç AH, İpek Y. Sonochemical Synthesis of Hydroxyapatite Nanoparticles with Different Precursor Reagents. *Acta Physica Polonica A* 2012;**121**(1):230-32.
47. Chow LC, Sun L, Hockey B. Properties of nanostructured hydroxyapatite prepared by a spray drying technique. *Journal of research of the National Institute of Standards and Technology* 2004;**109**(6):543.
48. Han J-K, Song H-Y, Saito F, Lee B-T. Synthesis of high purity nano-sized hydroxyapatite powder by microwave-hydrothermal method. *Materials Chemistry and Physics* 2006;**99**(2):235-39.
49. Qiu C, Xiao X, Liu R. Biomimetic synthesis of spherical nano-hydroxyapatite in the presence of polyethylene glycol. *Ceramics International* 2008;**34**(7):1747-51.
50. Wan Y, Huang Y, Yuan C, Raman S, Zhu Y, Jiang H, et al. Biomimetic synthesis of hydroxyapatite/bacterial cellulose nanocomposites for biomedical applications. *Materials Science and Engineering: C* 2007;**27**(4):855-64.
51. Tas AC. Synthesis of biomimetic Ca-hydroxyapatite powders at 37 C in synthetic body fluids. *Biomaterials* 2000;**21**(14):1429-38.
52. Thamaraiselvi T, Prabakaran K, Rajeswari S. Synthesis of hydroxyapatite that mimic bone minerology. *Trends Biomater Artif Organs* 2006;**19**(2):81-83.
53. Moshaverinia A, Ansari S, Moshaverinia M, Roohpour N, Darr JA, Rehman I. Effects of incorporation of hydroxyapatite and fluoroapatite nanobioceramics into conventional glass ionomer cements (GIC). *Acta Biomater* 2008;**4**(2):432-40.
54. Barnes DM, Blank LW, Gingell JC, GILNER PP. A clinical evaluation of a resin-modified: glass ionomer restorative material. *The Journal of the American Dental Association* 1995;**126**(9):1245-53.
55. Tyas MJ. Clinical evaluation of glass-ionomer cement restorations. *Journal of Applied Oral Science* 2006;**14**(SPE):10-13.
56. Barata TJE, Bresciani E, Adachi A, Fagundes TC, Carvalho CAR, Navarro MFL. Influence of ultrasonic setting on compressive and diametral tensile strengths of glass ionomer cements. *Materials Research* 2008;**11**(1):57-61.
57. Gu Y, Yap A, Cheang P, Khor K. Effects of incorporation of HA/ZrO 2 into glass ionomer cement (GIC). *Biomaterials* 2005;**26**(7):713-20.

58. Gu Y, Yap A, Cheang P, Koh Y, Khor K. Development of zirconia-glass ionomer cement composites. *Journal of non-crystalline solids* 2005;**351**(6):508-14.
59. Crisp S, Kent BE, Lewis BG, Ferner AJ, Wilson AD. Glass-ionomer cement formulations. II. The synthesis of novel polycarboxylic acids. *Journal of Dental Research* 1980;**59**(6):1055-63.
60. Yoon S, Lee YK, Kim YU, Kim MC, Kim KN, Kim S, et al. The effects of hydroxyapatite on bonding strength between dental luting cement and human teeth. Key Engineering Materials; 2005: Trans Tech Publ; 2005. p. 953-56.
61. Hesaraki S, Sharifi D, Nemati R, Nezafati N. Preparation and characterisation of calcium phosphate cement made by poly (acrylic/itaconic) acid. *Advances in Applied Ceramics* 2009;**108**(2):106-10.
62. Mohammed R, Raghad A. Assessment of consistency and compressive strength of glass ionomer reinforced by different amount of hydroxyapatite. *Scientific Journal Published by the*:16.
63. Hamilton I. Effects of fluoride on enzymatic regulation of bacterial carbohydrate metabolism. *Caries research* 1977;**11**(Suppl. 1):262-91.
64. Goenka S, Balu R, Kumar TS. Effects of nanocrystalline calcium deficient hydroxyapatite incorporation in glass ionomer cements. *Journal of the mechanical behavior of biomedical materials* 2012;**7**:69-76.
65. Ramli RA, Adnan R, Bakar MA, Masudi SaM. Synthesis and characterisation of pure nanoporous hydroxyapatite. *J Phys Sci* 2011;**22**(1):20-37.
66. Chen Y, Miao X. Thermal and chemical stability of fluorohydroxyapatite ceramics with different fluorine contents. *Biomaterials* 2005;**26**(11):1205-10.
67. Phillips MJ. Chemical coupling in biocomposites: surface modification of bioceramics creating chemically bound polymer composites with potential osteological applications: Queen Mary, University of London; 2005.
68. Chen M, Jiang D, Li D, Zhu J, Li G, Xie J. Controllable synthesis of fluorapatite nanocrystals with various morphologies: Effects of pH value and chelating reagent. *Journal of Alloys and Compounds* 2009;**485**(1):396-401.
69. Wei M, Evans J, Bostrom T, Grøndahl L. Synthesis and characterization of hydroxyapatite, fluoride-substituted hydroxyapatite and fluorapatite. *Journal of Materials Science: Materials in Medicine* 2003;**14**(4):311-20.
70. Montazeri N, Jahandideh R, Biazar E. Synthesis of fluorapatite–hydroxyapatite nanoparticles and toxicity investigations. *International journal of nanomedicine* 2011;**6**:197.
71. Suchanek W, Yoshimura M. Processing and properties of hydroxyapatite-based biomaterials for use as hard tissue replacement implants. *Journal of Materials Research* 1998;**13**(01):94-117.
72. Redey SA, Nardin M, Bernache–Assolant D, Rey C, Delannoy P, Sedel L, et al. Behavior of human osteoblastic cells on stoichiometric hydroxyapatite and type A carbonate apatite: role of surface energy. *J Biomed Mater Res* 2000;**50**(3):353-64.
73. Nikčević I, Jokanović V, Mitrić M, Nedić Z, Makovec D, Uskoković D. Mechanochemical synthesis of nanostructured fluorapatite/fluorhydroxyapatite and carbonated fluorapatite/fluorhydroxyapatite. *Journal of Solid State Chemistry* 2004;**177**(7):2565-74.
74. Milne K, Calos N, O'DONNELL J, KENNARD CL, Vega S, Marks D. Glass-ionomer dental restorative: Part I: a structural study. *Journal of Materials Science: Materials in Medicine* 1997;**8**(6):349-56.
75. Cefaly DFG, Valarelli FP, Seabra BGdM, Mondelli RFL, Navarro MFdL. Effect of time on the diametral tensile strength of resin-modified restorative glass ionomer cements and compomer. *Braz Dent J* 2001;**12**(3):201-4.
76. Yap A, Pek Y, Kumar R, Cheang P, Khor K. Experimental studies on a new bioactive material: HAIonomer cements. *Biomaterials* 2002;**23**(3):955-62.

77. Lin J, Zhu J, Gu X, Wen W, Li Q, Fischer-Brandies H, et al. Effects of incorporation of nano-fluorapatite or nano-fluorohydroxyapatite on a resin-modified glass ionomer cement. *Acta Biomater* 2011;**7**(3):1346-53.
78. Bhattacharjee P, Begam H, Chanda A. Development and physical, chemical and mechanical characterization of doped hydroxyapatite. *International Journal of Scientific & Engineering Research* 2011;**2**(4):1-8.
79. Sidhu SK, Watson TF. Resin-modified glass ionomer materials. A status report for the American Journal of Dentistry. *American Journal of Dentistry* 1995;**8**(1):59-67.
80. Mohammadi Basir M, Ataei M, Bagher Rezvani M, Golkar P. Effect of incorporation of various amounts of nano-sized hydroxyapatite on the mechanical properties of resinmodified glass ionomer. *Beheshti Univ Dent J* 2013;**4**:216-23.

Figure captions

Figure 1. XRD patterns of the HA and FA nanoparticles after calcination in the air at 20 °C, 600 °C, 700 °C and 800 °C for 1h

Figure 2. FTIR spectra of the HA and FA nanoparticles after calcination in the air at 700 ºC for 1h

Figure 3. The SEM micrographs of the HA and FA nanoparticles after calcinations at 700 °C

Figure 4. The TEM micrographs of the HA and FA nanoparticles after calcinations at 700 °C

Figure 5. The SAED pattern of the HA and FA nanoparticles after calcinations at 700 °C

Figure 6. XRD patterns of Fuji II GIC (a), HA-added GIC (b) and FA-added GIC (c) after mixing with poly acid

Figure 7. (a) Back scatter and (b) Secondary electron SEM micrographs of the GIC containing HA nanoparticles

Figure 8. (a) Back scatter and (b) Secondary electron SEM micrographs of the GIC containing FA nanoparticles

Figure 9. Compressive strength of GIC, 5 wt% HA and 5 wt% FA-added GIC after 1, 7 and 28 days storage in distilled water at 37 ºC

Figure 10. Compressive strength of GIC, 8 wt% HA and 8 wt% FA-added GIC after 1, 7 and 28 days storage in distilled water at 37 ºC

Figure 11. Diametral tensile strength of GIC, 5 wt% HA and 5 wt% FA-added GIC after 1, 7 and 28 days storage in distilled water at 37 ºC

Figure 12. Diametral tensile strength of GIC, 8 wt% HA and 8 wt% FA-added GIC after 1, 7 and 28 days storage in distilled water at 37 ºC

Tables

Table 1. Lattice parameters and crystallite size of the synthesized HA and FA nanoaprticles

Sample	a (Å)	b (Å)	c (Å)	Crystal size (nm)	Crystal instructure
HA	9.4328	9.4328	6.88	16.9	hexagonal
FA	9.367	9.367	6.88	22.5	hexagonal

Table 2. Ca and P content in the synthesized HA nanoparticles and Ca/P ratio

Sample	Element	Amount at (700 º C)	Amount at (800 º C)	Ca/P (700°C)	Ca/P (800 °C)
HA	Ca	39.1	37.65	1.665	1.59
	P	18.5	18.5		

Table 3. Ca and P content in the synthesized FA nanoparticles and Ca/P ratio

Sample	Element	Amount at (700 º C)	Amount at (800 º C)	Ca/P (700°C)	Ca/P (800 °C)
FA	Ca	39.6	39.3	1.65	1.635
	P	18.6	18.61		

Table 4. BET analysis of synthesized HA and FA nanoparticles

Sample	BET (m^2/g)
HA	31.99
FA	26.95

Table 5. Setting and working time of the GIC and modified GIC

Sample	Setting time (s)±SD	Working time (s)±SD
GIC	340±37	235±16
GIC+ 5% HA	295±28	215±21

GIC+ 5% FA	275±22	210±28
GIC+ 8% HA	215±25	198±34
GIC+ 8% FA	225±31	198±29

Table 6. Micro hardness of the GIC and modified GIC at 37 ºC after 1 day and 7 days storing in distilled water

Sample	Hardness after 1 day (VHN)±SD	Hardness after 7 days (VHN)±SD
GIC	79±8.42	158±14.79
GIC+ 5% HA	85.8±6.71	161.5±10.43
GIC+ 5% FA	86.1±8.24	176.6±11.16
GIC+ 8% HA	89.5±8.08	168±9.92
GIC+ 8% FA	121.2±13.79	201±10.04

Figures

Figure 1

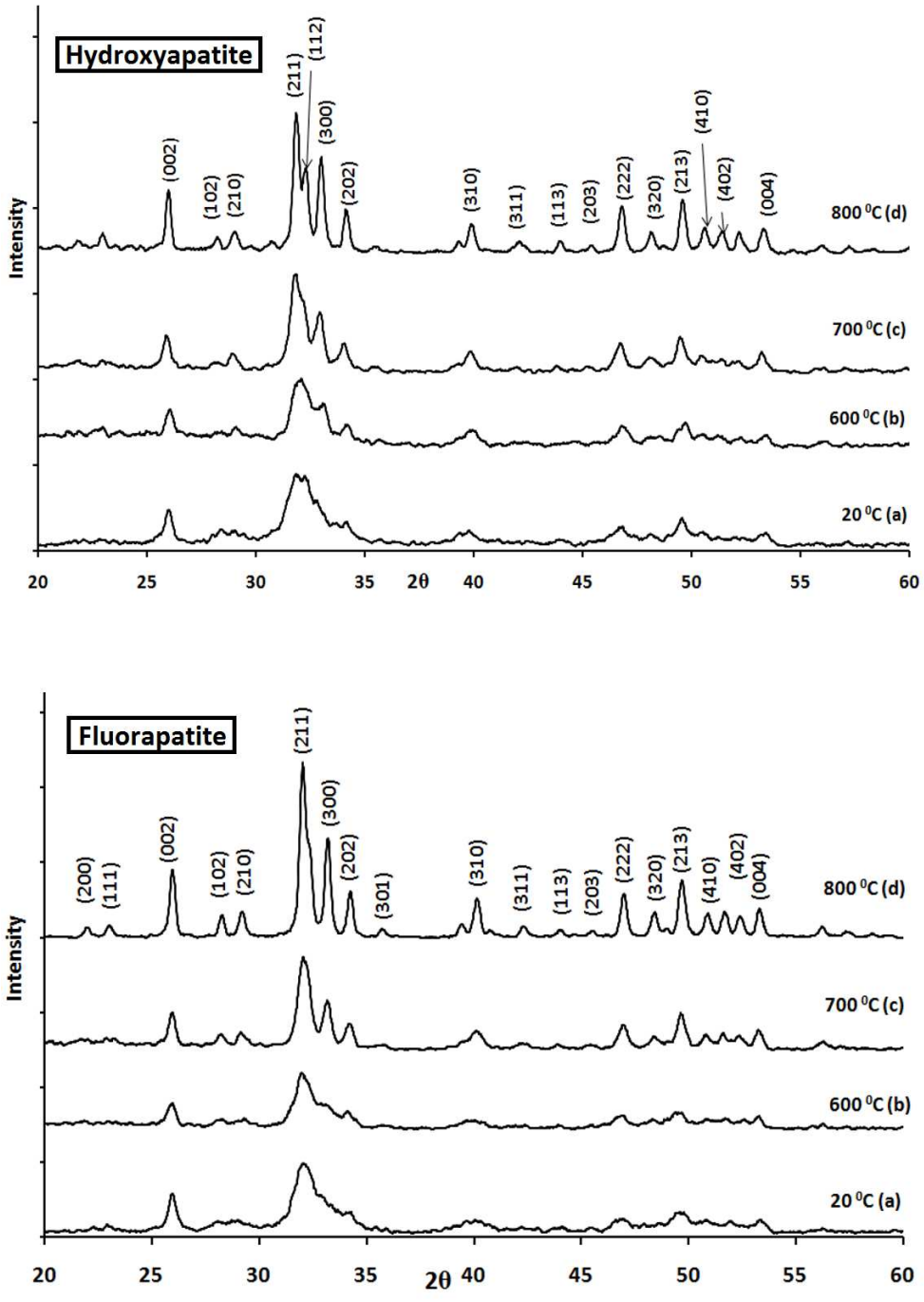

Figure 2

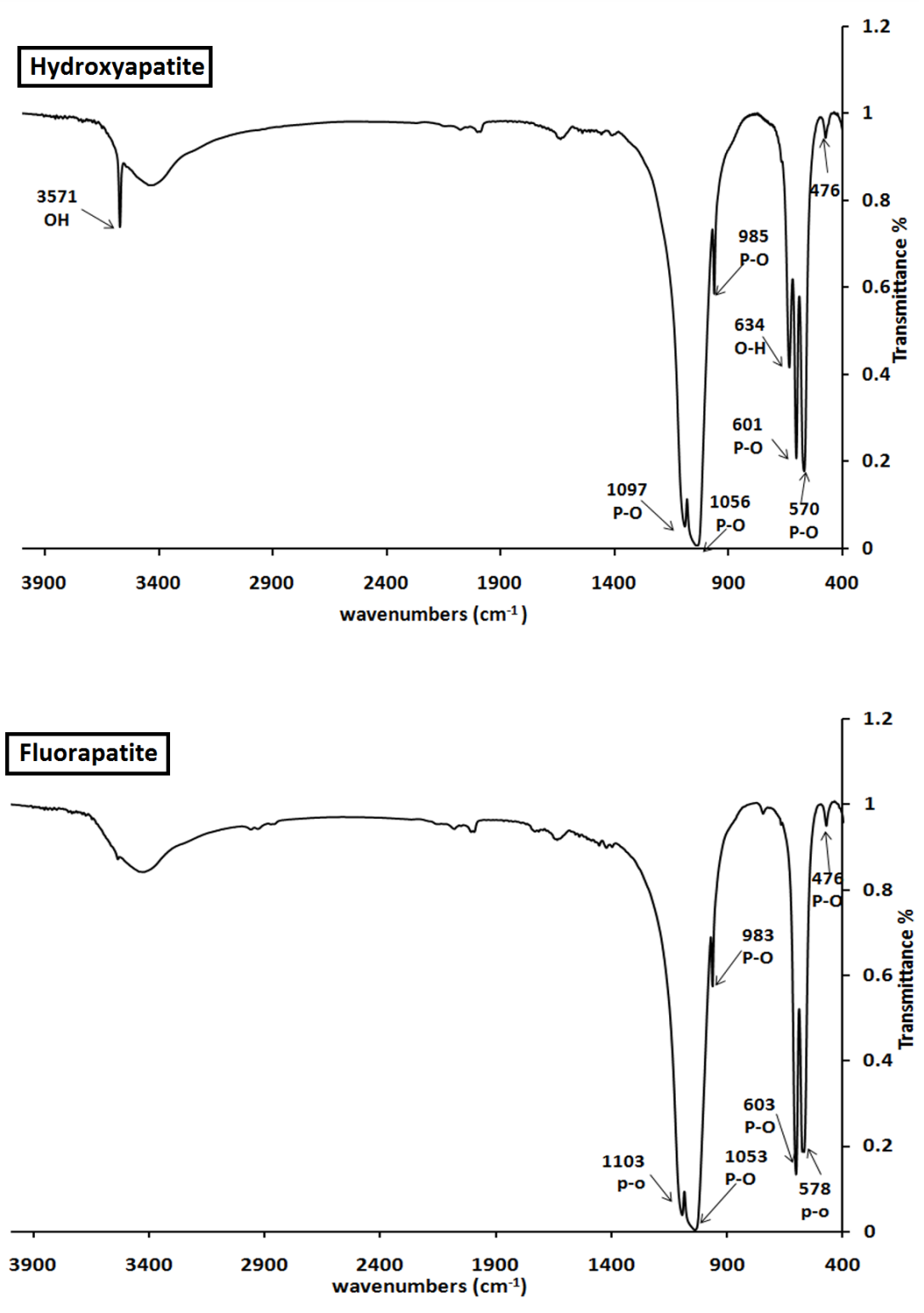
Hydroxyapatite
3571
OH
985
P-O
634
O-H
601
P-O
476
1097
P-O
1056
P-O
570
P-O
Transmittance %
wavenumbers (cm-1)
Fluorapatite
476
P-O
983
P-O
603
P-O
1103
p-o
1053
P-O
578
p-o
Transmittance %
wavenumbers (cm-1)

Figure 3

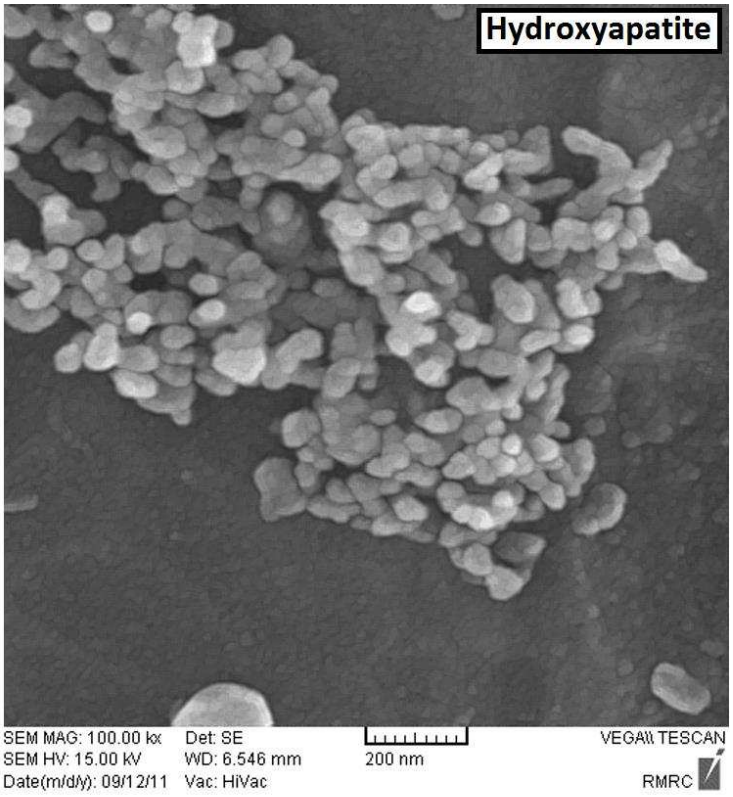
Hydroxyapatite
SEM MAG: 100.00 kx
SEM HV: 15.00 kV
Date(m/d/y): 09/12/11
Det: SE
WD: 6.546 mm
Vac: HiVac
200 nm
VEGA\\ TESCAN
RMRC

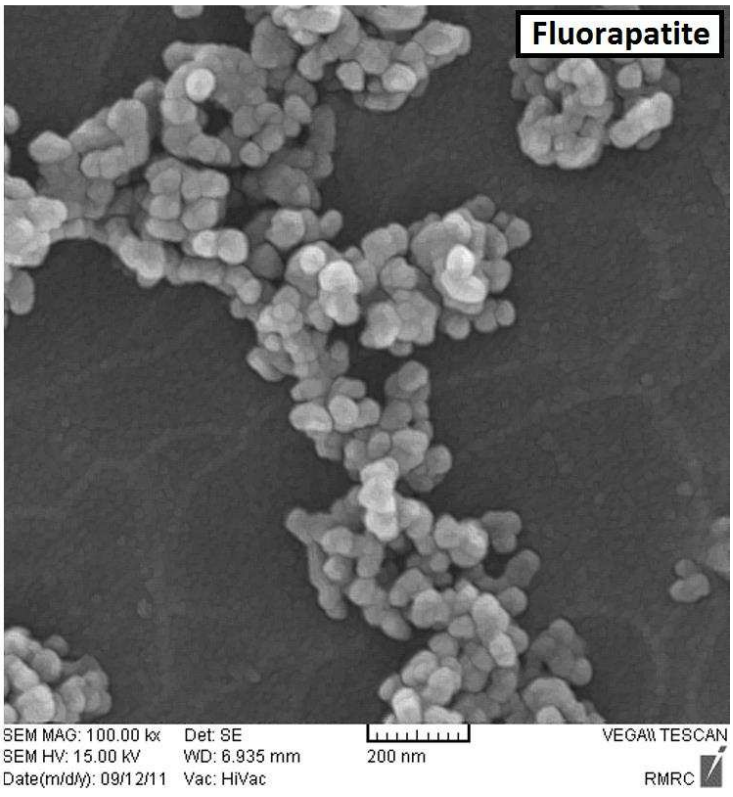
Fluorapatite
SEM MAG: 100.00 kx
SEM HV: 15.00 kV
Date(m/d/y): 09/12/11
Det: SE
WD: 6.935 mm
Vac: HiVac
200 nm
VEGA\\ TESCAN
RMRC

Figure 4

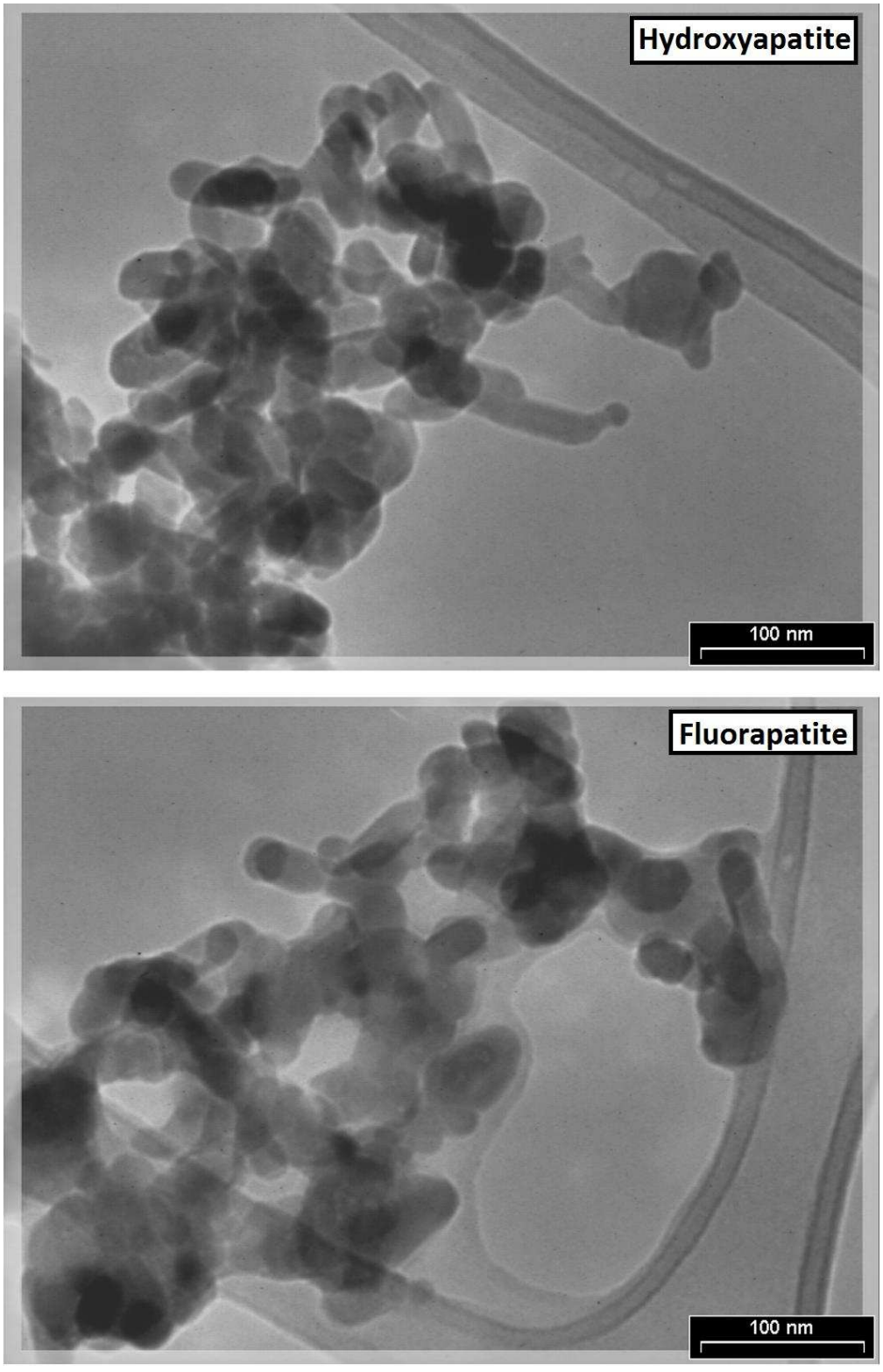

Figure 5

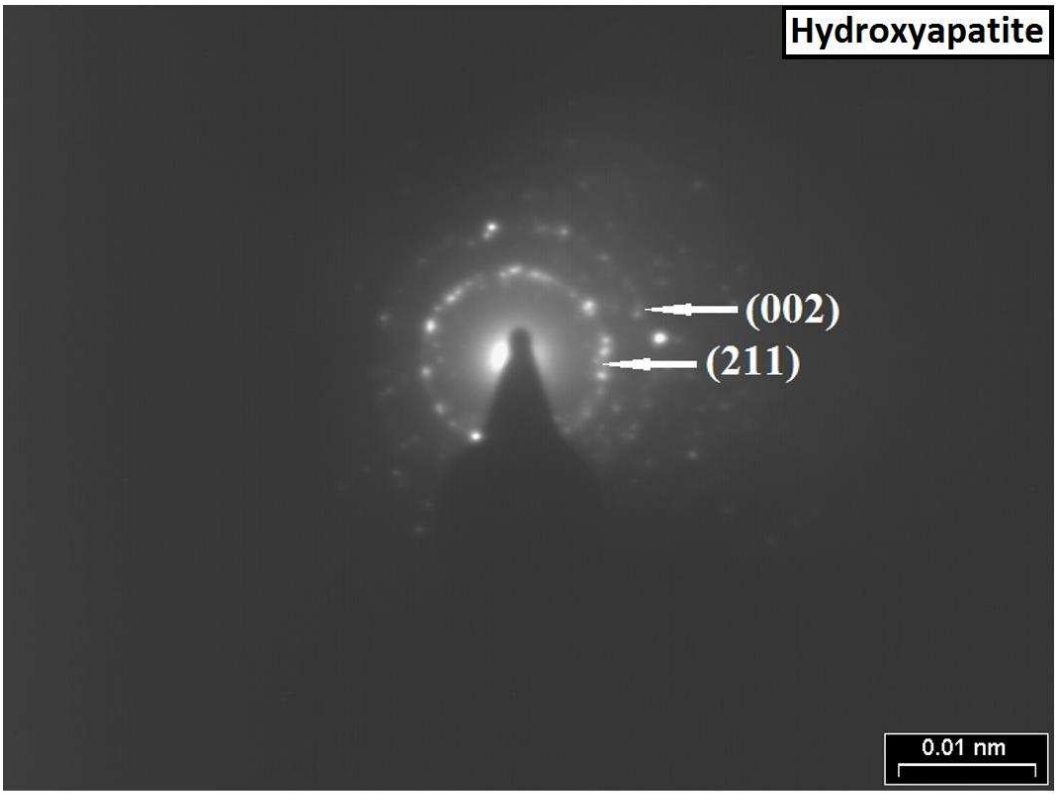
Hydroxyapatite
(002)
(211)
0.01 nm

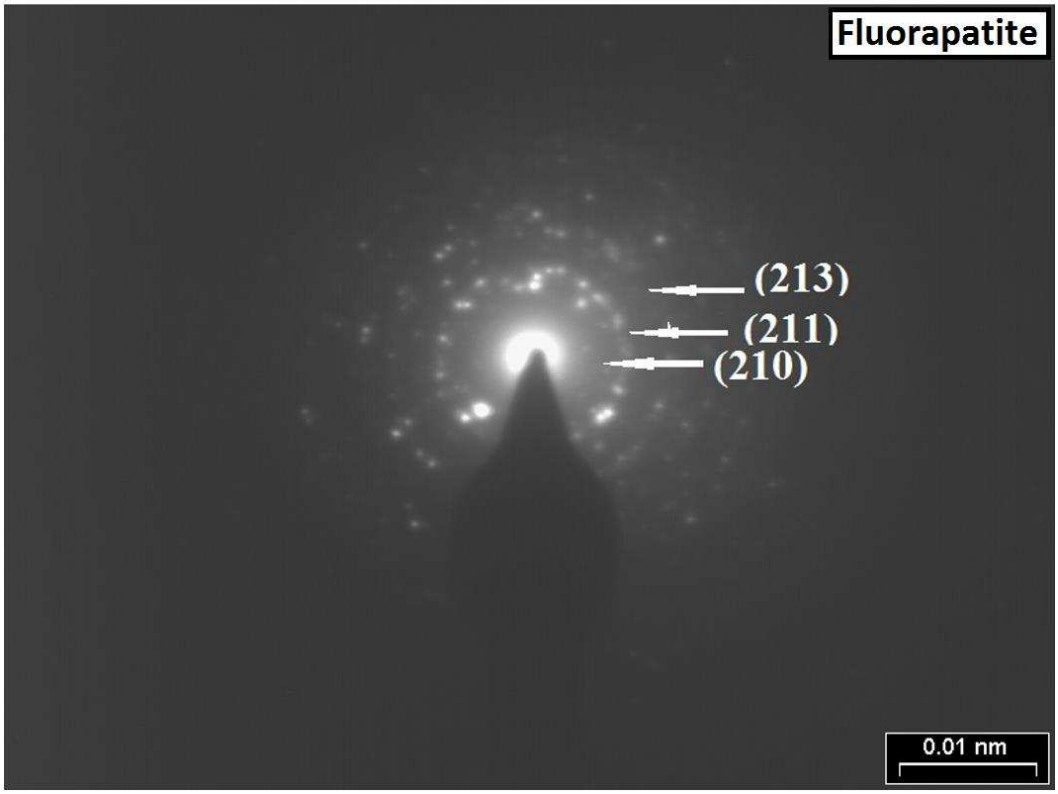
Fluorapatite
(213)
(211)
(210)
0.01 nm

Figure 6

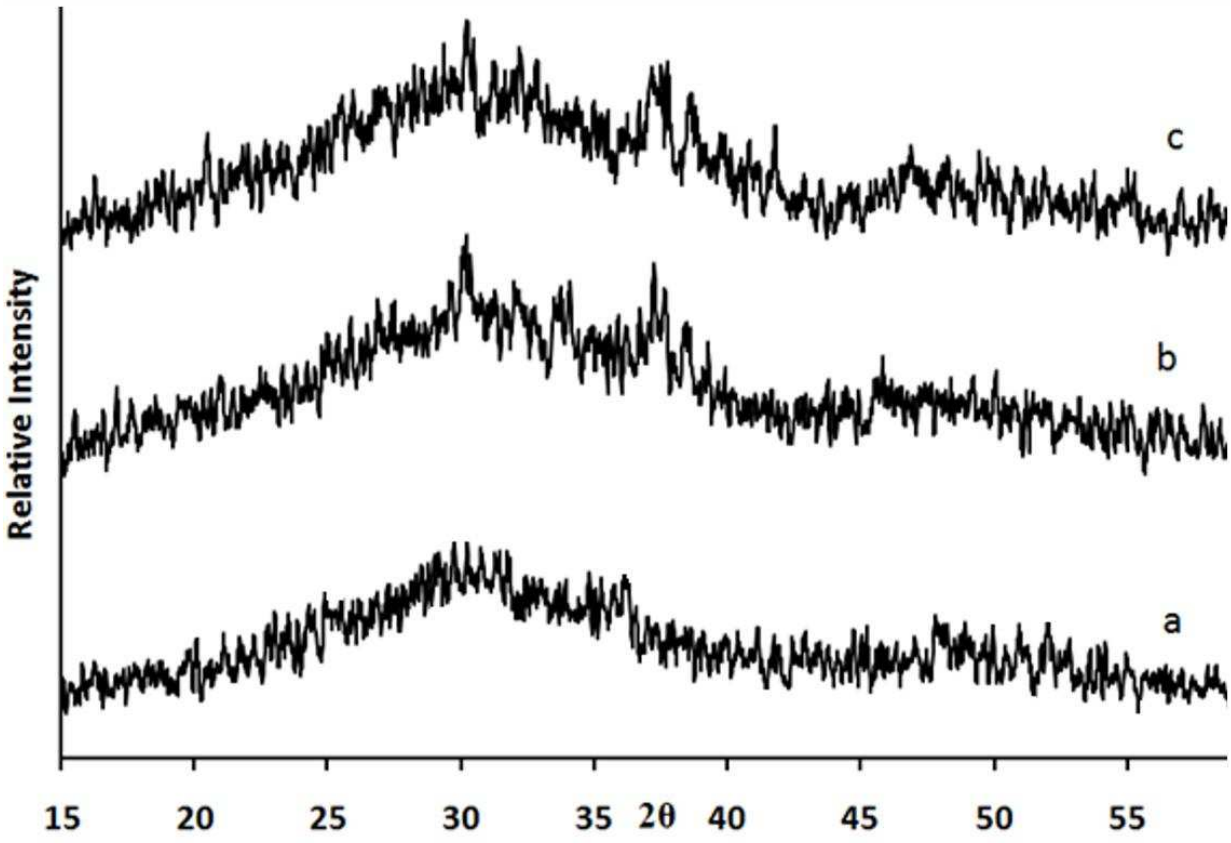

Figure 7

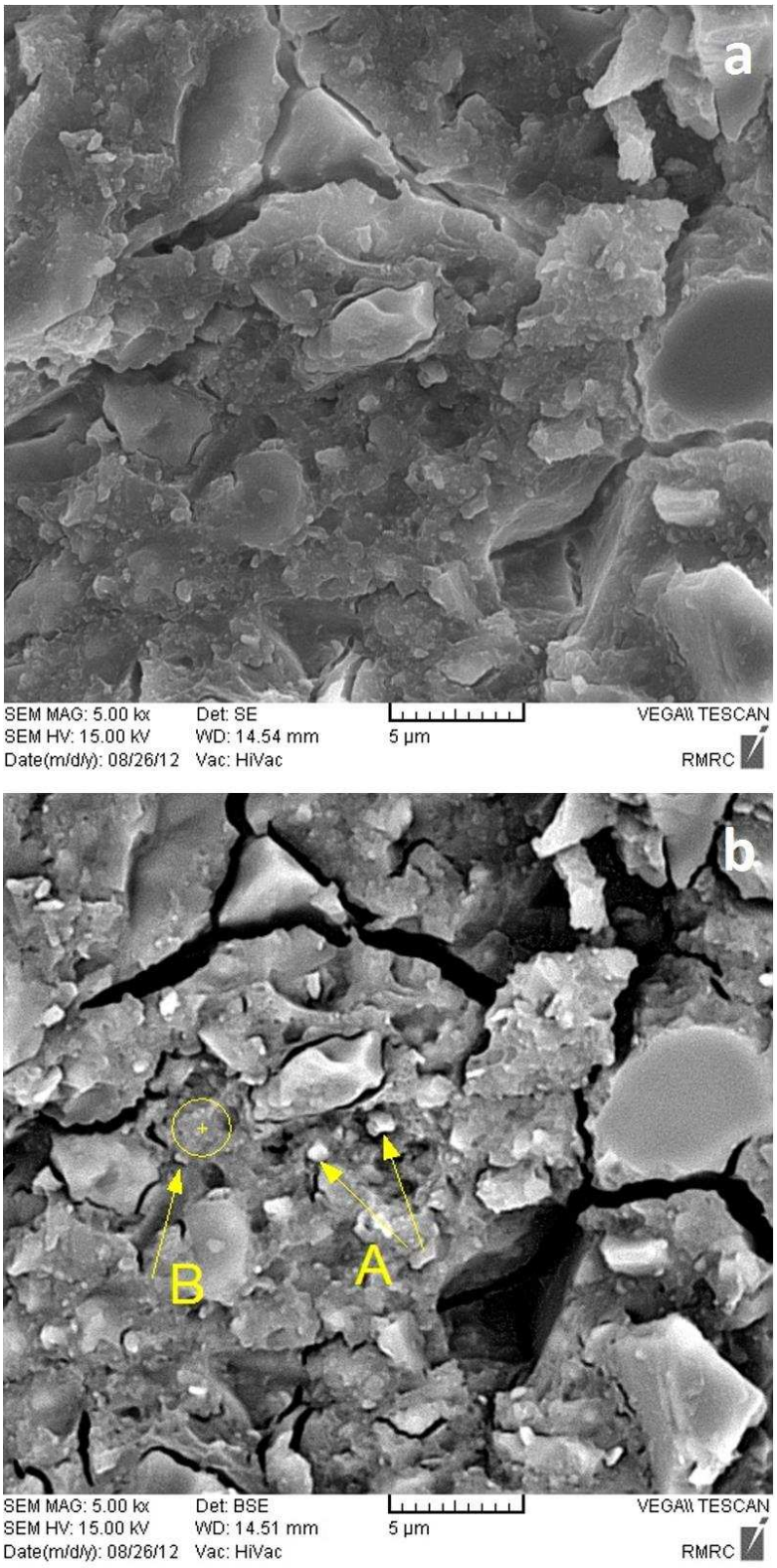
a
SEM MAG: 5.00 kx
SEM HV: 15.00 kV
Date(m/d/y): 08/26/12
Det: SE
WD: 14.54 mm
Vac: HiVac
5 µm
VEGA\\ TESCAN
RMRC
b
B
A
SEM MAG: 5.00 kx
SEM HV: 15.00 kV
Date(m/d/y): 08/26/12
Det: BSE
WD: 14.51 mm
Vac: HiVac
5 µm
VEGA\\ TESCAN
RMRC

Figure 8

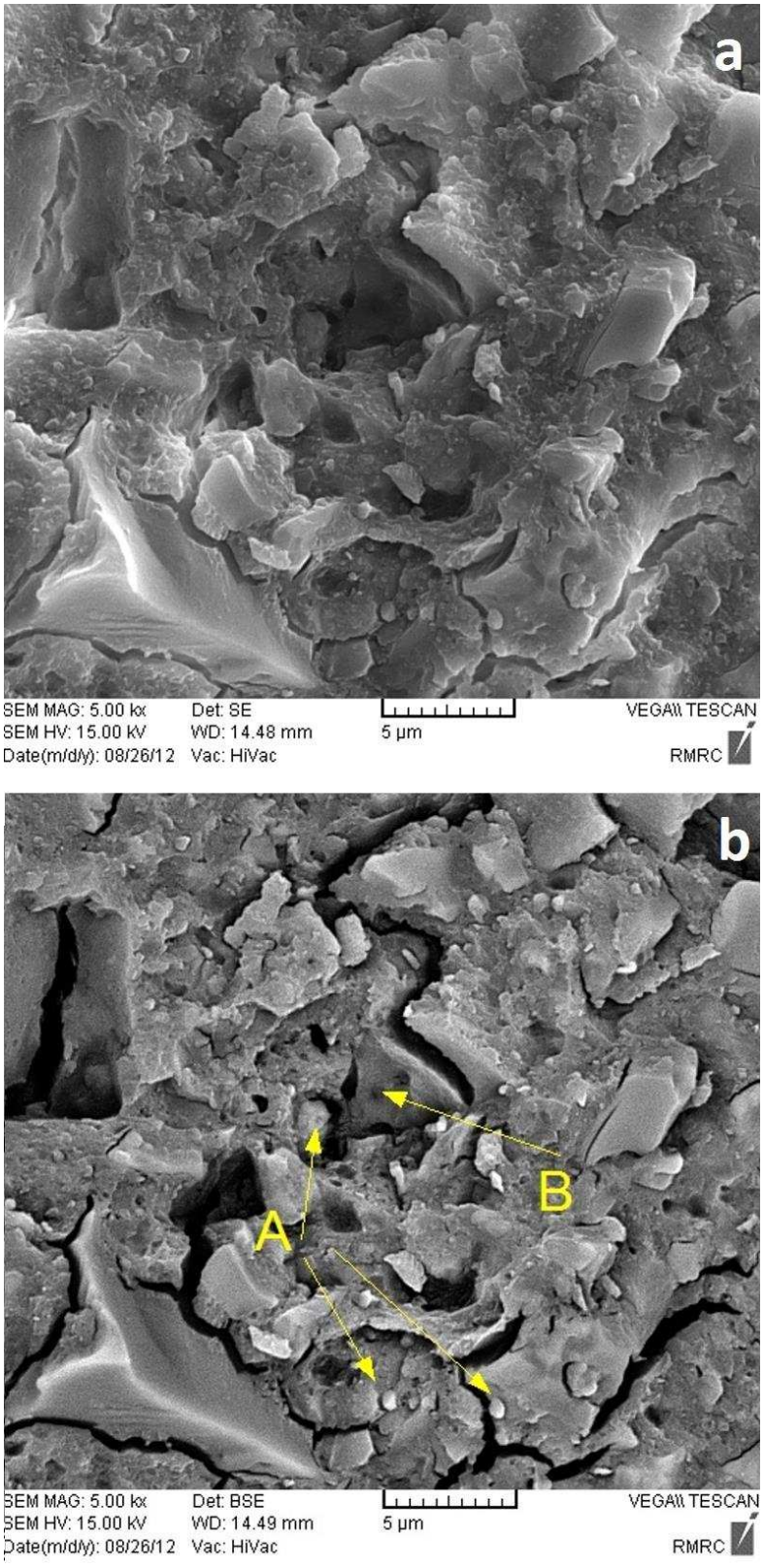
a
SEM MAG: 5.00 kx
SEM HV: 15.00 kV
Date(m/d/y): 08/26/12
Det: SE
WD: 14.48 mm
Vac: HiVac
5 µm
VEGA\\ TESCAN
RMRC
b
A
B
SEM MAG: 5.00 kx
SEM HV: 15.00 kV
Date(m/d/y): 08/26/12
Det: BSE
WD: 14.49 mm
Vac: HiVac
5 µm
VEGA\\ TESCAN
RMRC

Figure 9

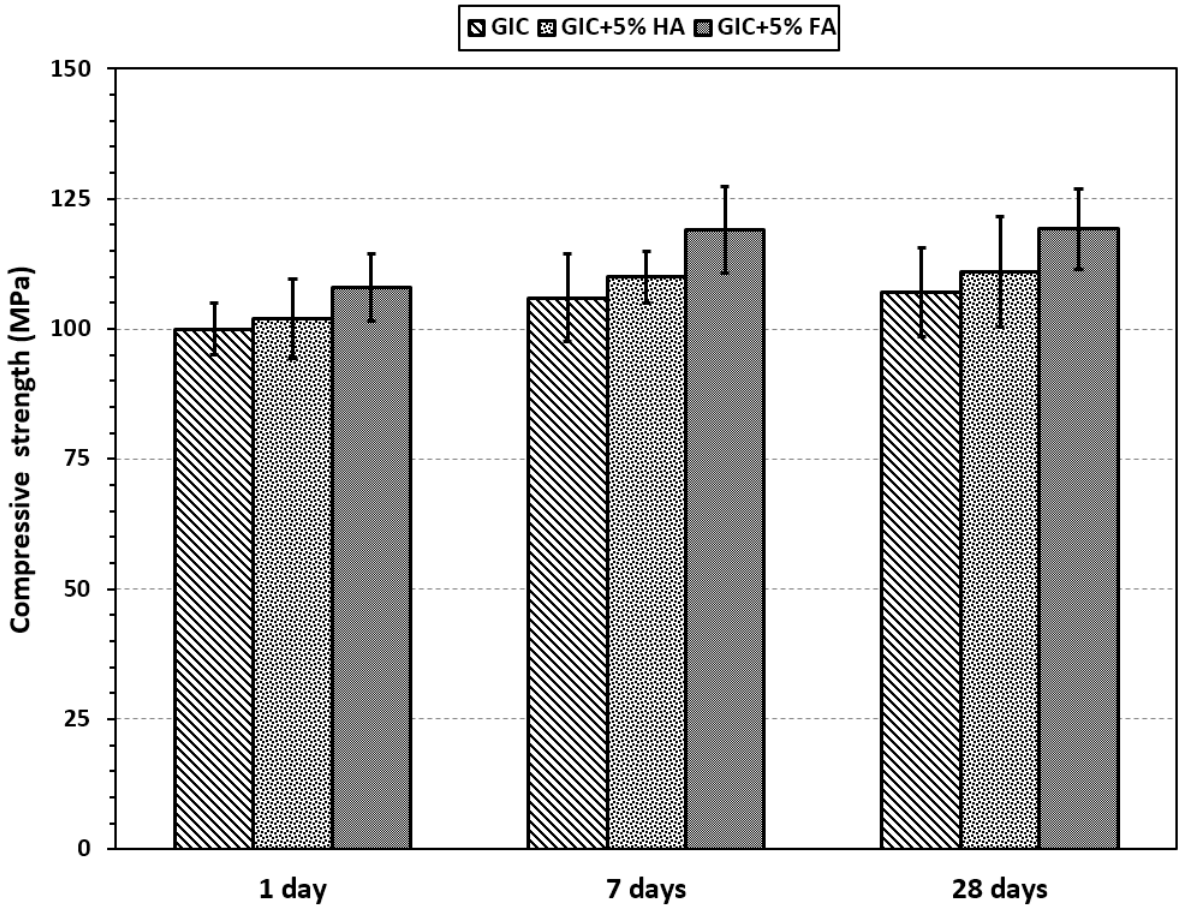
GIC
GIC+5% HA
GIC+5% FA
Compressive strength (MPa)
150
125
100
75
50
25
0
1 day
7 days
28 days

Figure 10

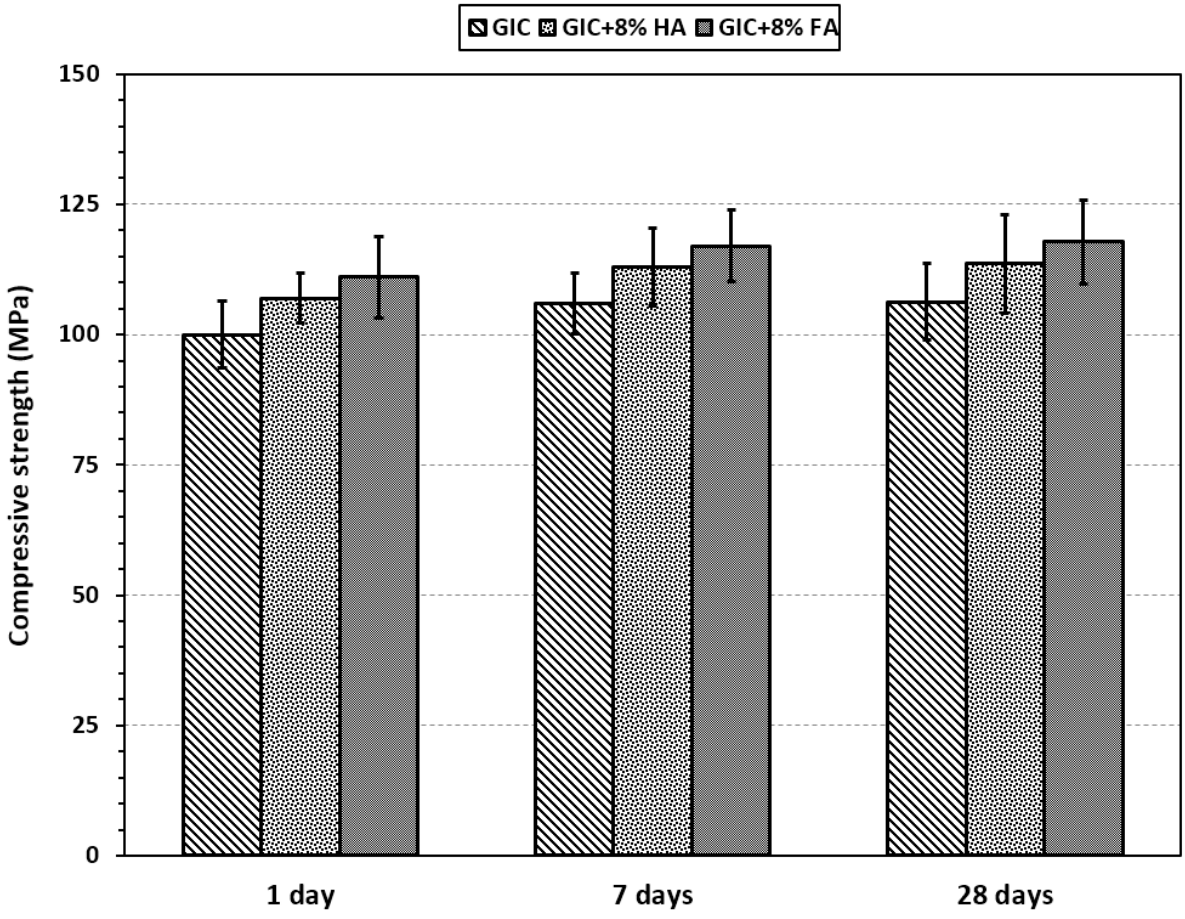
GIC
GIC+8% HA
GIC+8% FA
Compressive strength (MPa)
150
125
100
75
50
25
0
1 day
7 days
28 days

Figure 11

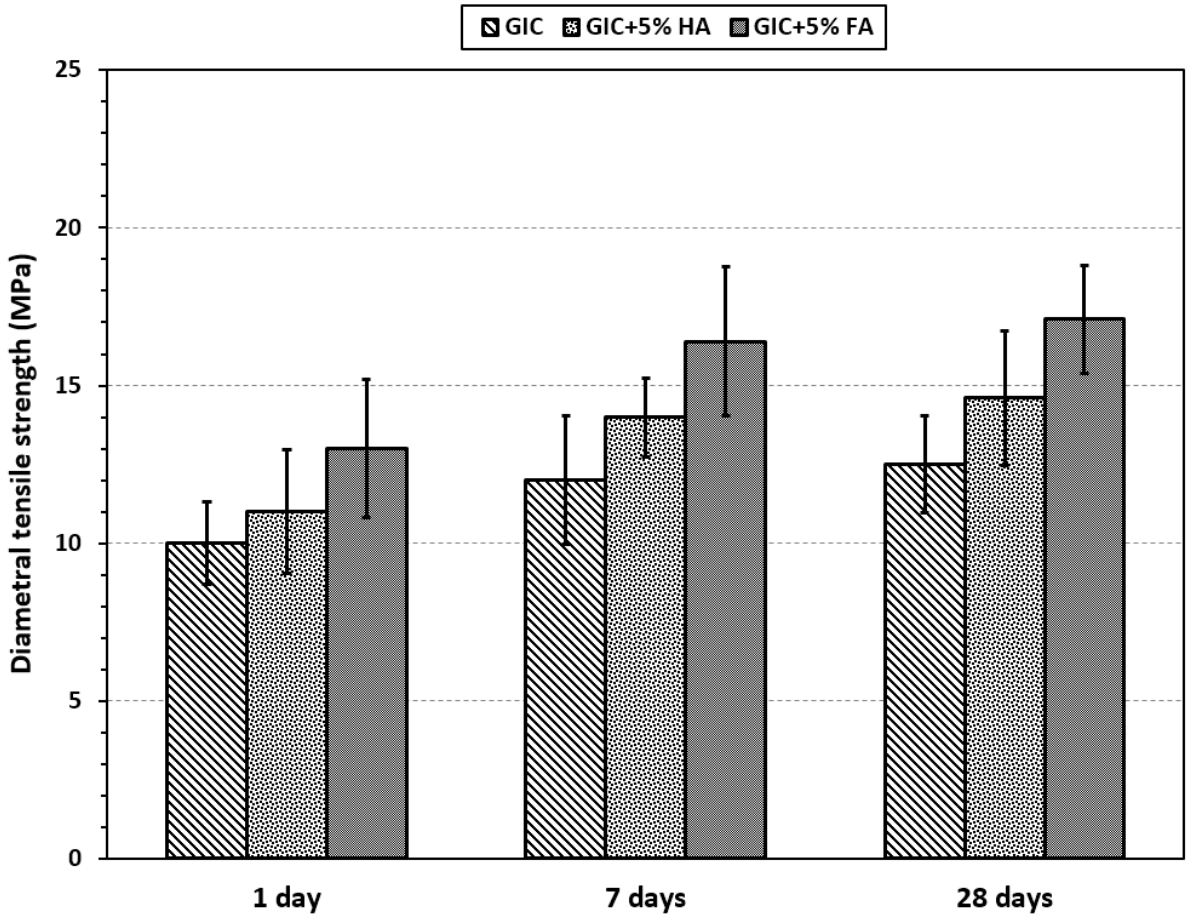
GIC
GIC+5% HA
GIC+5% FA
Diametral tensile strength (MPa)
25
20
15
10
5
0
1 day
7 days
28 days

Figure 12

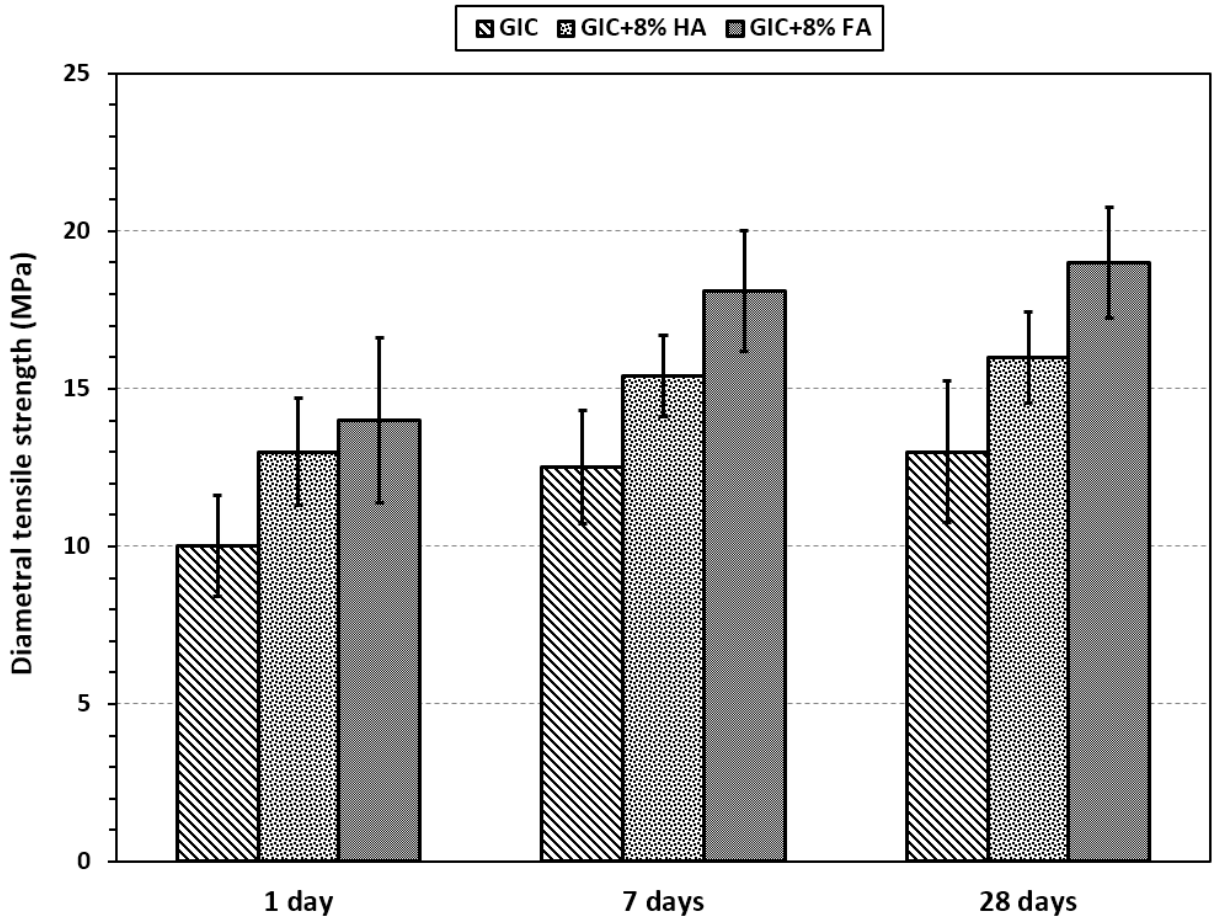
GIC
GIC+8% HA
GIC+8% FA
Diametral tensile strength (MPa)
25
20
15
10
5
0
1 day
7 days
28 days